Advancing DIA-based Limited Proteolysis Workflows: introducing DIA-LiPA

Chloé Van Leene[1,2‡], Emin Araftpoor[1,2‡], An Staes[1,2,3], Andrea Argentini[1,2], Marcel Bühler[1,2], Kris Gevaert[1,2*]

[1] VIB UGent Center for Medical Biotechnology, VIB, B9052 Ghent, Belgium

[2] Department of Biomolecular Medicine, Ghent University, B9052 Ghent, Belgium

[3] VIB Proteomics Core, B9052 Ghent, Belgium

‡ Authors contributed equally to this work

* Correspondence to: kris.gevaert@vib-ugent.be

Abstract

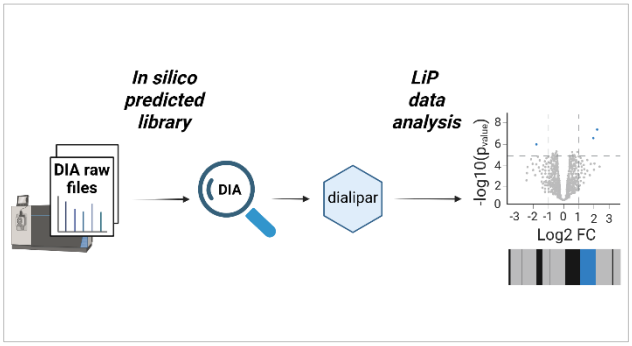

Limited proteolysis coupled to mass spectrometry (LiP-MS) probes protein conformational dynamics, but interpretation of LiP-MS data is complicated by heterogenous proteolytic cleavage patterns and missing data. Recent advances in data-independent acquisition (DIA) and machine learning-based search engines promise improved sensitivity and reproducibility, yet their performance in LiP-MS workflows remains underexplored. We systematically evaluated selected library-free DIA workflows using a rapamycin-treated human cell lysate and a yeast heat shock dataset, benchmarking DIA-NN and Spectronaut for identification depth, reproducibility and false discovery rate control. Our results show that library-free approaches achieve high sensitivity, eliminating the experimental overhead and sample requirements associated with empirical libraries. Building on these advances, we introduce a DIA-based Limited Proteolysis data Analysis pipeline (DIA-LiPA), a data analysis workflow tailored for LiP-MS data that integrates semi-tryptic- and tryptic-level precursor data and accounts for missingness to enable structural interpretation. Validation across multiple datasets confirmed that DIA-LiPA reproduces known structural signatures and uncovers additional regulatory patterns, providing a robust framework for mechanistic insights into protein dynamics.

Introduction

Protein functions are tightly determined by their structures. Instead of having a single, static form, proteins adopt various conformational states, known as conformational ensembles, that may change in response to environmental stimuli, ligand binding or post-translational modifications[1]. Such conformational changes are strongly linked to alterations in protein functions and, for example, regulate protein-protein interactions [2,3]. Therefore, understanding protein conformational dynamics helps elucidating cellular processes and disease mechanisms [1,4].

Structural proteomics aims to characterize conformational changes and several mass spectrometry-based techniques have been developed for this purpose, including cross-linking mass spectrometry (XL-MS) [5,6], hydrogen-deuterium exchange mass spectrometry (HDX-MS) [7], thermal proteome profiling (TPP) [8,9], peptide-centric local stability assay (PELSA) [10] and limited proteolysis coupled to mass spectrometry (LiP-MS)[11]. While XL-MS and HDX-MS provide valuable insights into protein-protein interactions and solvent accessibility, respectively, their proteome-wide application remains technically challenging due to sample complexity, data analysis and limited coverage of the proteins and structural regions accessible to these methods [12]. TPP and its more recent derivative PISA (Proteome Integral Solubility Assay) measure changes in protein stability upon perturbation, though do not directly provide conformational information [12–14]. PELSA, a more recent limited-proteolysis-based strategy uses high concentrations of trypsin to sensitively detect ligand-induced local stability shifts. This enables identification of ligand-binding regions and their corresponding proteins. While conceptually similar to LiP-MS, PELSA is less sensitive in pinpointing exact binding sites and conformational changes at the peptide level [10].

Among these techniques, LiP-MS stands out for its ability to probe conformational changes in complex samples. It relies on the principle that a protein's conformation determines those sites at its surface that will be cleaved by a protease, and such sites are found in solvent-exposed and flexible protein regions. Conformational changes altering protease access to these regions thus result in distinct protease cleavage patterns. In LiP-MS, proteins are first briefly incubated with a promiscuous protease (e.g., proteinase K), followed by complete digestion with trypsin. This results in so-called conformotypic peptides, a term that encompasses both newly formed semi-tryptic and tryptic peptides whose abundance is affected by structural rearrangements. Conformational peptides thus serve as structural fingerprints of a protein. By now comparing

proteolytic LiP signatures across conditions, such as drug or metabolite binding, LiP-MS enables the detection of conformational changes at peptide level and the identification of functionally relevant protein regions [11,15,16].

Initially, LiP-MS workflows employed Data-Dependent Acquisition (DDA) to identify conformotypic peptides and build spectral libraries for downstream analysis. DDA only selects and fragments the most abundant peptide ions, hereafter referred to as precursors, and its stochastic precursor selection leads to missing values and thus limited reproducibility in complex samples. To overcome these limitations, Data-Independent Acquisition (DIA) has been increasingly adopted. Unlike DDA, DIA systematically fragments all precursors within defined mass windows, enabling more comprehensive and reproducible peptide quantification. DIA workflows in LiP-MS are often supported by project-specific spectral libraries generated from DDA runs, which provide deep coverage, especially when peptides were pre-fractionated prior to DDA. However, generating such libraries is time-consuming, requires additional sample material and remains subject to DDA's inherent biases.

The semi-tryptic nature of LiP-MS data has also posed challenges for library-free DIA approaches, given the increased spectral complexity and expanded search space [17–19]. Recent advances in machine learning and deep neural networks have addressed these issues. Tools like DIA-NN [20] and Spectronaut [21] now enable accurate precursor identification and quantification directly from DIA LiP-MS data, without the need for experimental spectral libraries. These tools can predict precursor fragmentation patterns and retention times with high precision, enabling library-free workflows that match and even exceed the sensitivity and reproducibility of traditional DDA-based approaches [18,20]. DIA-NN, uses a peptide-centric approach to identify candidate precursors, followed by a spectrum-centric strategy to resolve interference from co-eluting peptides [20]. In contrast, Spectronaut uses a spectrum-centric approach by generating DDA-like pseudo-MS/MS spectra, which can be searched using conventional DDA search engines.

However, false discovery rate (FDR) control remains a challenge in DIA workflows, particularly in conformational proteomics applications like LiP-MS, where it is important to distinguish subtle conformational changes from background variation and analytical noise [19,22]. In DIA, such noise can arise from the co-isolation and co-fragmentation of multiple precursors within the same selection window, leading to inference from co-eluting peptides and increased spectral complexity

[17]. This challenge is further amplified in LiP-MS by the inclusion of semi-tryptic peptides, which increase peptide-level complexity and expand the search space. As a result, FDR estimation becomes more difficult, with the search space inflating up to 20-fold compared to tryptic searches, thereby increasing the likelihood of identifying false positives [17]. While DDA-based libraries help control the FDR by constraining the search space, library-free approaches rely on the discriminative power of deep learning to more effectively distinguish true from false positives.

To overcome the limitations of DDA-based library generation and address the specific challenges of LiP-MS data, we developed DIA-LiPA, a flexible and comprehensive pipeline tailored for DIA-based Limited Proteolysis data Analysis. DIA-LiPA operates on precursor-level quantification outputs from DIA-NN or Spectronaut and performs data filtering, abundance normalization and differential abundance analysis, ultimately generating interpretable outputs such as volcano plots and structural barcodes with missingness information included. The pipeline, implemented in an open-source R package dialipar[a], is compatible with both Spectronaut and DIA-NN, and adaptable to various experimental designs. Despite the fact that the recent release of DIA-NN's beta version[b] includes the semi-tryptic option, DIA-LiPA was initially developed in the context of a semi-tryptic FASTA-based workaround in DIA-NN, hence we also incorporated this approach into our study. Notably, several pipelines or software packages have been proposed for LiP-MS data analysis, including protti [23], MSstatsLiP [16] and LiPAnalyzeR [24], each offering tailored approaches for peptide-level quantification and structural interpretation. However, none of these currently support DIA-NN output or report missingness patterns, which are key features addressed by DIA-LiPA.

In this study, we use DIA-LiPA as a unified downstream analysis pipeline to systematically compare traditional LiP-MS acquisition workflows, including DDA-based spectral libraries and library-free approaches in both DIA-NN (version 2.3) and Spectronaut (version 19). Our results demonstrate that in our datasets, focused on LiP-MS and semi-tryptic peptide analysis, library-free workflows perform comparably or better than DDA-based library methods. This suggests that empirical libraries may not be strictly necessary for these types of applications. Importantly, DIA-LiPA allows for the interpretation of missingness patterns, which are biologically relevant in LiP-

[a] https://github.com/Gevaert-Lab/dialipar

[b] https://github.com/vdemichev/DiaNN/releases/tag/2.0

MS. Structural changes may completely prevent the generation of specific semi-tryptic peptides, resulting in condition-specific absence that reflects conformational rearrangements rather than technical noise. Furthermore, by not restricting the analysis to fully tryptic peptides, DIA-LiPA provides a more comprehensive and robust view of conformational dynamics, capturing abundance changes, shifts in proteolytic accessibility and allowing mutual validation between peptide types.

Materials and methods

Cell Culture and Proteome Preparation

HEK293T cells were cultured in Dulbecco's Modified Eagle Medium (DMEM; Gibco), supplemented with 10% fetal bovine serum (FBS; Gibco) under standard conditions (37 °C, 5% CO_2). After several passages, cells were harvested by trypsinization, followed by neutralization with complete DMEM. The cell suspension was centrifuged at 450 *g* for 3 min at room temperature. The supernatant was aspirated and the pellet was washed with phosphate-buffered saline (PBS), followed by a second centrifugation under the same conditions. After removal of the supernatant, the resulting cell pellet was snap-frozen in liquid nitrogen and stored at -80 °C until further use.

A cell pellet equivalent to approximately 12 million HEK293T cells was lysed using a pellet pestle motor (Kimble®) in 300 µL of LiP buffer (100 mM HEPES, pH 7.4; 150 mM KCl; 1 mM $MgCl_2$). Lysis was performed on ice with 10 pulses every minute for 10 min. The lysate was then centrifuged at 16000 *g* for 10 min at 4 °C, and the supernatant was transferred to a fresh microcentrifuge tube (Eppendorf, 1.5 mL). Protein concentration was determined using the Pierce BCA Protein Assay Kit (Thermo Scientific), following the manufacturer's instructions.

Limited Proteolysis (LiP) Treatment

The cell lysate was divided into two conditions: a trypsin control (TC) sample, subjected to only trypsin digestion, and a LiP sample, subjected to double-protease digestion with proteinase K followed by complete trypsin digestion. Each sample contained 50 µg of lysate.

The LiP protocol [16] was performed as follows: samples were incubated at 25 °C for 5 min, followed by treatment with either 10 µM rapamycin (Sigma-Aldrich) in 0.1% dimethyl sulfoxide (DMSO; Sigma-Aldrich) or 0.1% DMSO as vehicle control, at 25 °C for 5 min. Proteinase K (PK; Promega) was then added to the LiP samples at an enzyme-to-substrate ratio of 1:100 (w/w) and incubated at 25 °C for 5 min. For the control samples, an equivalent volume of water was added instead of PK.

Proteolysis was stopped by heating the samples at 99 °C for 5 min, followed by cooling at 4 °C for 5 min. Deoxycholate (DOC; Sigma-Aldrich) was then added to a final concentration of 5%.

Trypsin Digestion and Peptide Preparation

Samples were reduced with 5 mM tris-(2-carboxyethyl)phosphine (TCEP, Thermo Scientific) at 37 °C for 30 min, and alkylated with 40 mM iodoacetamide (Sigma-Aldrich) at 30 °C for 30 min in the dark. Samples were diluted with 0.1 M ammonium bicarbonate (Merck) to reduce the DOC concentration to 1%.

Sequencing Grade Modified Trypsin (Promega) was added at an enzyme-to-substrate ratio of 1:100 (w/w) and incubated overnight at 37 °C in a thermomixer at 800 rpm. Digestion was stopped by acidifying the samples to pH < 2 with 50% formic acid.

Peptides were desalted using Microspin C18 columns (Nest Group), eluted with 50% acetonitrile and 0.1% formic acid, dried in a vacuum centrifuge and stored at -20 °C.

High-pH Reversed-Phase Fractionation of Peptides

Peptides were reconstituted in 20 µL loading solvent A (0.1% trifluoroacetic acid in water/acetonitrile (ACN) (98:2, v/v)). LiP and control replicates (16 µL per sample, 4 replicates per condition) were pooled separately, yielding approximately 50 µg of total peptide digest per condition. Each pooled sample was dried down, reconstituted in fractionation solvent A (10 mM ammonium acetate pH 5.5 in H_2O) and fractionated into 12 pooled fractions using high-pH reversed-phase chromatography on a Vanquish™ Flex (Thermo Fisher Scientific) equipped with a Zorbax 300SB-C18 column (0.3 × 150 mm, 3.5 µm; Agilent) preceded by a Zorbax 300SB-C18 guard cartridge (0.5 x 5 mm, 5 µm; Agilent).

Separation was performed using a 100-minute linear gradient from 1 to 100% acetonitrile (ACN) at a flow rate of 8 µl/min. Peptide elution was monitored with 1-min fractions collected from 50 to 148 min and online pooled every 12 min. After vacuum drying, the individual fractions were resuspended in loading solvent A' (0.5% ACN in 0.1% trifluoroacetic acid (TFA)), spiked with Biognosys' iRT kit peptides according to the manufacturer's instructions.

Online Liquid Chromatography

Peptides were reconstituted in 20 µL loading solvent A (0.1% trifluoroacetic acid in water/acetonitrile (ACN) (98:2, v/v)). For each injection, either 2 µL of unfractionated, unpooled

sample (for DIA) or 10 µl of fractionated, pooled sample (for DDA) was injected on an Ultimate 3000 Pro Flow nanoLC system in-line connected to a Q Exactive HF mass spectrometer (Thermo). Trapping was performed at 20 µl/min for 2 min in loading solvent A on a 5 mm trapping column (Thermo scientific, 300 µm internal diameter (i.d.), 5 µm beads). The peptides were separated on a 250 mm Aurora Ultimate analytical column (1.7 µm C18, 75 µm i.d.; Ionopticks) kept at a constant temperature of 45 °C in a butterfly oven (Phoenix S&T). Peptides were eluted by a non-linear gradient starting at 0.5% MS solvent B (0.1% FA in acetonitrile) reaching 26% MS solvent B in 75 min, 44% MS solvent B in 95 min, 56% MS solvent B in 100 min followed by a 5-minute wash at 56% MS solvent B and re-equilibration with MS solvent A (0.1% FA in water) at a constant flowrate of 250 nl/min.

DIA Acquisition

Unfractionated, unpooled peptides were analysed in data-independent acquisition (DIA) mode, automatically switching between MS and MS/MS acquisition. Full-scan MS spectra ranging from 375-1,500 m/z with a target value of 5E6, a maximum fill time of 50 ms and a resolution of 60,000 were followed by 30 quadrupole isolations with a precursor isolation width of 10 m/z for HCD fragmentation at an NCE of 30% after filling the trap at a target value of 3E6 for maximum injection time of 45 ms. MS2 spectra were acquired at a resolution of 15,000 at 200 m/z in the Orbitrap analyser without multiplexing. The isolation intervals ranging from 400-900 m/z of 10 m/z were created with the Skyline software tool. QCloud was used to control instrument longitudinal performance during the project [25,26].

DDA Acquisition for Spectral Library Generation

Pooled, fractionated peptides were analysed in data-dependent acquisition (DDA) mode, automatically switching between MS and MS/MS acquisition for the 12 most abundant ion peaks per MS spectrum. Full-scan MS spectra (375-1,500 m/z) were acquired at a resolution of 60,000 in the Orbitrap analyzer after accumulation to a target value of 3E6 with a maximum ion time of 60 ms. The 12 most intense ions above a threshold value of 1.3E4 were isolated (isolation window of 1.5 m/z) for fragmentation at a normalized collision energy of 30% after filling the trap at a target value of 1E5 for maximum 80 ms. MS/MS spectra (with a fixed first mass of 145 m/z) were acquired at a resolution of 15,000 in the Orbitrap analyzer. The polydimethylcyclosiloxane

background ion at 445.120028 Da was used for internal calibration (lock mass) and QCloud has been used to control instrument longitudinal performance during the project [25,26].

Mass Spectrometry Data Analysis

DIA raw files were searched in two different ways: (1) library-free using *in silico* predicted spectral libraries, and (2) empirical library-based using spectral libraries generated from DDA analysis of offline peptide fractions.

Library-free (in silico predicted) DIA

DIA data were analysed using Spectronaut (version 19.9; Biognosys AG) [21] and DIA-NN (version 2.3) [20] (Table 1).

In both tools, semi-specific digestion was applied to enable the identification of semi-tryptic peptides directly from DIA data. Notably, semi-specific digestion was only recently introduced in DIA-NN (version 2.3); earlier versions required a semi-tryptic FASTA workaround (see Supporting Information). For DIA-NN, the scoring strategy was set to Proteoforms. Both tools used the human UniProt FASTA (01/2024) supplemented with the proteinase K (*Tritirachium album*) sequence. Search parameters were harmonized across tools and included missed cleavages 1, charge states 1 to 4, peptide length 7 to 30 amino acids, fragment ion m/z range 200 to 2,000, maximum number of variable modifications 1, oxidation (M) as variable modification, carbamidomethylation (C) as fixed modification and N-terminal methionine excision disabled. All other settings were kept at default values.

To further demonstrate the applicability and usefulness of the DIA-LiPA pipeline, we reanalysed a yeast heat shock dataset (PRIDE accession: PXD022297) [27] using library-free DIA in both Spectronaut and DIA-NN. To ensure comparability with the original publication, we employed the same *S. cerevisiae* (strain S288c) UniProt FASTA (11/2016).

Empirical library-based DIA

Offline DDA fractionation data were analysed using either Spectronaut Pulsar (version 19.9) or FragPipe (version 23) using MSFragger version 4.3 [28] for spectral library generation (Table 1). To ensure a clean comparison with the library-free DIA searches, the same search parameters were

applied as described above. These libraries were then used to search the DIA data using Spectronaut and DIA-NN (version 2.3) (Table 1).

In Spectronaut, spectral libraries were generated using Pulsar with the same UniProt FASTA (supplemented with the proteinase K sequence). LiP samples were searched using semi-specific digestion and trypsin-control samples with specific digestion.

In FragPipe, the DIA-SpecLib-Quant workflow was used to build spectral libraries from DDA files. The same FASTA file was used as in Spectronaut supplemented with the Biognosys iRT peptide sequences, with cleavage set to SEMI for LiP samples and ENZYMATIC for trypsin-control samples. In the Spec Lib tab, RT calibration was set to Biognosys_iRT and psm.tsv was selected as the Filetype to Convert.

Table 1: Overview of different data analysis tools and settings used in this study.

	Tool	Version	Digestion setting	Library size (if applicable)	Notes
In silico predicted library	Spectronaut	19.9	Semi-specific	/	
	DIA-NN	2.3	Semi	65,119,115 precursors	Semi-option newly available in this version.
	DIA-NN	2.2	/	47,923,754 precursors	Library generated from semi-tryptic FASTA; semi-specific digestion not yet supported.
Empirical library generation	Spectronaut Pulsar	19.9	Semi-specific (LiP) / Specific (TC)	/	Libraries used in Spectronaut.
	MSFragger (FragPipe)	4.3 (23)	SEMI (LiP) / ENZYMATIC (TC)	/	DIA-SpecLib-Quant workflow; libraries used in DIA-NN.
Empirical library search	Spectronaut	19.9	Semi-specific (LiP) / Specific (TC)	47,044 (LiP) / 51,377 (TC) precursors	
	DIA-NN	2.3	Semi	49,301 (LiP) / 48,823 (TC) precursors	

Entrapment to Assess False Discovery Rate (FDR)

To assess FDR control in the library-free approaches, the *E. coli* proteome (08/2025) was included as an entrapment database alongside the previously mentioned human proteome database. Because the entrapment database is smaller than the human proteome database, the combined estimation method was applied, which accounts for the ratio r of entrapment to target database sizes [22]. The estimated FDR was calculated as:

$$FDR = \frac{N_\varepsilon(1 + 1/r)}{N_\tau + N_\varepsilon}$$

where N_τ and N_ε denote the number of precursors identified from the human and entrapment (*E. coli*) databases, respectively.

DIA-LiPA Statistical Method Description

Precursors with a valid MS2-based quantity (Precursor.Quantity > 0 in DIA-NN or FG_MS2RawQuantity > 4 in Spectronaut) are filtered to retain those with at least two identifications per sample group. For example, a precursor with three measurements in group A and one in group B, will only be filtered out of group B. Precursors that can be the product of tryptic digestion are annotated as tryptic, those that either end on or are preceded by lysine or arginine as semi-tryptic, and others as non-tryptic. Precursors that are not proteotypic or repeat within a protein sequence are annotated within each sequence context separately. Within each pipeline, i.e., limited proteolysis (LiP) or trypsin-control (TC), data are normalised separately by subtracting a sample-specific scaling factor from all $\log_2$ precursor quantities. This scaling factor is calculated using only the precursors that are shared between all samples in a pipeline (i.e., complete cases) and equals the $\log_2$ difference between the sample median and the pipeline-wide median. Following normalisation, coverages are calculated on a protein accession level. Sample correlations are calculated based on the complete precursors using the Spearman correlation, and the principal component analysis is similarly performed using the complete cases using singular value decomposition. For differential abundance analysis on the LiP precursors, protein group-level abundance adjustment factors are first derived from the TC samples by aggregating complete precursors to protein groups using robust summarisation using the normalised $\log_2$ precursor quantities. Protein groups aggregated from fewer than two precursors are discarded. The scaling

factor is then calculated as the difference between the median protein group-level quantity of each sample group from the median across all TC samples. For the TC-adjustment, this protein-group- and condition-level scaling factor is then subtracted from the normalised log2 precursor quantity of all precursors mapping to the corresponding protein group in the LiP samples. Subsequently, quantitative modelling is performed using msqrob2, and again non-proteotypic and repeating precursors are deconcatenated for downstream reporting and visualisation. A schematic overview of these steps is provided in the dashed box in **Figure 1**.

All steps above are part of the dialipar[c] R package, which includes a report generation layer based on Quarto. The html report generated includes several QC plots, and for each contrast a volcano plot of the differential analysis with a barcode for the proteins of interest.

The raw files, search results, FASTA files and all data analysis scripts and outputs underlying this study have been deposited to MassIVE (MSV000099740) and will be made publicly available upon acceptance of the manuscript.

[c] https://github.com/Gevaert-Lab/dialipar

Results and Discussion

Experimental design for performance assessment in DIA-based LiP-MS

To evaluate the performance of our newly developed pipeline, DIA-LiPA, we used a target-engagement LiP-MS experiment in which cell lysates were treated with either rapamycin or a solvent control. Rapamycin is a well-characterized small molecule known to selectively bind FKBP1A [29], making it an ideal molecule to assess the sensitivity and specificity of different LiP-MS workflows. LiP-MS was performed following established protocols [30,31], and the resulting data were analysed using four DIA workflows: (i) empirical library search in Spectronaut or (ii) in DIA-NN, and (iii) library-free search in Spectronaut ("directDIA") or (iv) in DIA-NN. Downstream analysis of all four workflows was performed using DIA-LiPA (**Figure 1**). For the first two workflows, we fractionated peptides using high-pH reverse-phase chromatography, followed by DDA acquisition of the resulting fractions. The acquired DDA data were then searched using either Spectronaut Pulsar or FragPipe, and the resulting identifications were used to construct a project-specific spectral library for subsequent DIA analysis. This approach integrates peptide fragmentation and retention time data, thereby restricting DIA searches to a predefined precursor list. These libraries were then used to search the DIA data using either Spectronaut or DIA-NN (**Figure 1**, grey). Peptide fractionation prior to DDA acquisition is a common practice to enhance spectral library coverage. While not explicitly included in the original LiP-MS protocol [16], this step substantially increases the number of identifiable precursors, resulting in a 3.5 to 4 times larger spectral library compared to the unfractionated counterpart.

In contrast, the library-free approach bypasses the need for prior DDA runs by predicting spectral libraries *in silico* from a protein FASTA file. This allows for less biased analysis of the DIA data. We implemented this strategy using Spectronaut's directDIA mode and DIA-NN's newly introduced semi-specific digestion feature (**Figure 1**, blue). Other LiP-MS analysis packages, such as LiPAnalyzer and MSstatsLiP, were considered but not included in our benchmarking due to incompatibility with DIA-NN outputs and data processing steps that are less accessible and more convoluted. Such constraints prevent a fair comparison under the conditions evaluated in this study.

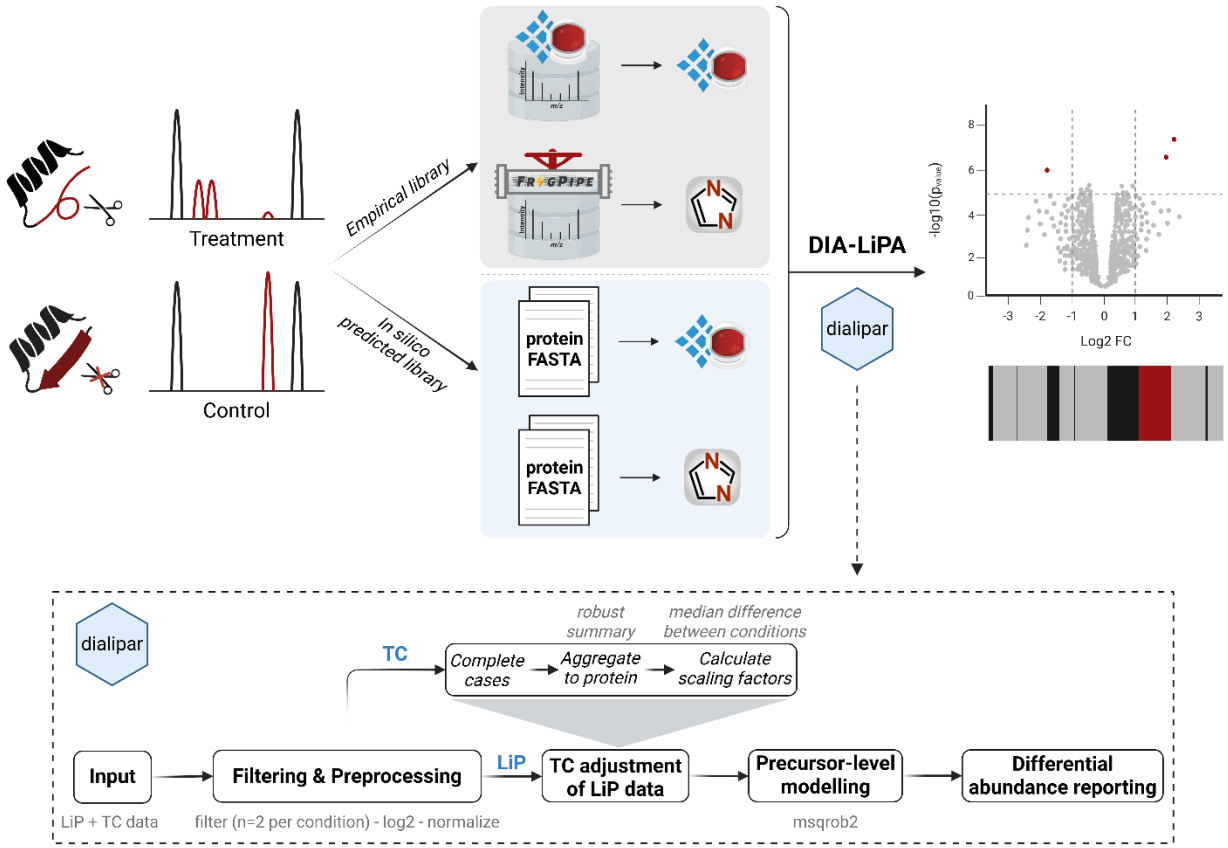

Figure 1: Experimental setup and DIA LiP-MS workflows analysed with DIA-LiPA. A treatment-control LiP-MS experiment was performed using cell lysates treated with either rapamycin or solvent control. The resulting data were analysed using four DIA LiP-MS workflows: grey indicates workflows using empirical DDA-based libraries, blue indicates workflows using *in silico* predicted libraries. Downstream analysis was performed with DIA-LiPA to identify significant conformational changes across the proteome, with its stepwise workflow outlined in the dashed box and implemented in the *dialipar* R package. The scissors icon represents limited proteolysis with proteinase K. Figure created with BioRender.com. LiP-MS; limited proteolysis coupled to mass spectrometry, TC; trypsin control, DDA; data-dependent acquisition, DIA; data-independent acquisition.

Precursor-level identifications, coverage and reproducibility across DIA workflows in LiP-MS

We first assessed the number of identified precursors and the proportion of semi-tryptics across the different DIA workflows (**Figure 2A**). Library-free workflows identified approximately three times more precursors than empirical library-based workflows, while maintaining the expected proportion of semi-tryptics (25-30%) typical for LiP-MS experiments. Although peptide fractionation was performed to mitigate DDA stochasticity and enhance library depth,

identification rates remained lower than those achieved with library-free DIA. Within the library-free approaches, DIA-NN showed slightly higher sensitivity for semi-tryptics (33%) compared to Spectronaut (28%). Furthermore, we observed a substantial overlap between library-free workflows, and about 60% of the precursors identified in empirical library-based workflows were also found in library-free workflows. This suggests that a considerable number of precursors are shared, yet many remain unique to each approach. Given that library-free workflows identified three times more precursors overall, they offer broader coverage of the proteome.

To further evaluate proteome coverage, we compared the sequence coverage of shared proteins (**Figure 2B**). Library-free workflows achieved broader and more consistent coverage, due to the detection of low-abundant and semi-tryptic peptides that are often missed in empirical DDA-based libraries. As shown in the overlap panels, the choice of search engine (Spectronaut versus DIA-NN) did not appear to have a major impact on overall coverage, suggesting that differences are primarily driven by the type of library used. This enhanced coverage is particularly beneficial for LiP-MS, where it translates to improved structural resolution and enables the detection of subtler conformational changes. Similar trends were observed for non-shared proteins (**Figure S1A**), with library-free approaches reaching slightly higher coverages.

Semi-tryptic searches expand the search space over 15-fold compared to fully tryptic searches [32,33], which increases the identification rates but also introduces more false positives [34]. To confirm that the increased sensitivity of the library-free workflows reflects true identifications, we performed an entrapment experiment by adding the *E. coli* proteome to the human protein sequence database for a semi-tryptic search. The FDR was estimated using the combined entrapment method [22], which accounts for the database size differences and provides a conservative upper bound. The resulting FDR values, 0.53% for DIA-NN and 0.39% for Spectronaut (Table S1), indicate effective FDR control in semi-tryptic DIA analysis. These findings demonstrate that the library-free workflows have surpassed empirical library-based approaches in terms of sensitivity and coverage in LiP-MS experiments, reinforcing their applicability in structural proteomics and aligning with recent benchmarking studies [35].

We also assessed quantitative precision by comparing precursor-level coefficients of variation (CVs) of shared precursors across workflows (**Figure 2C**). CV distributions were similar across workflows, with Spectronaut CVs being slightly higher than DIA-NN. All workflows achieved

median CVs close to or below 20%, generally considered acceptable for quantitative proteomics [36]. In LiP-MS, semi-tryptics arise from non-canonical cleavage events by PK and occur at a lower abundance than standard tryptic peptides [37], leading to lower signal to noise ratios and in turn reducing quantitative precision. These factors explain why semi-tryptic workflows often exhibit broader CV distributions. Similar observations were made for non-shared precursors (**Figure S1B**), which showed slightly higher CVs overall, with Spectronaut exhibiting a bigger CV spread compared to DIA-NN. Furthermore, normalization strategies had a substantial impact on quantitative precision (**Figure S2**). Non-normalized data showed markedly higher CVs (often > 30%), underscoring the necessity of normalization for reliable quantification. Applying normalization reduced CVs to acceptable limits across all workflows, while additional trypsin-control (TC) adjustment did not alter results substantially, likely due to the nature of the rapamycin treatment in cell lysates, which is not expected to affect overall protein abundance. Achieving CVs close to or lower than 20% and maintaining FDR control is therefore particularly noteworthy, as it underscores the reliability of library-free DIA workflows, which combine high sensitivity with robust quantification while eliminating the experimental overhead of empirical library generation.

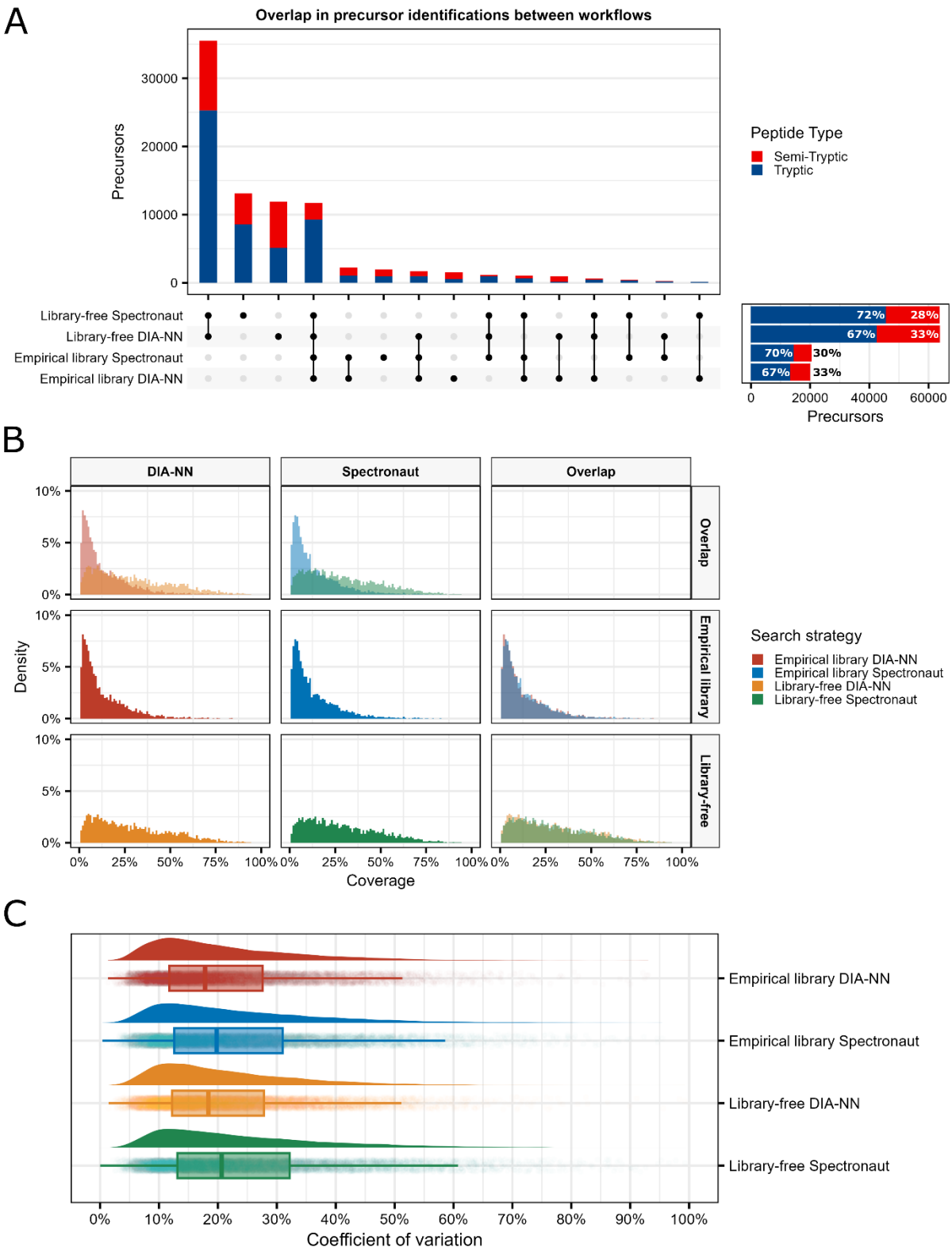

Figure 2: Comparison of identification, coverage and quantification precision across DIA workflows. A) UpSet plot showing the absolute number of precursors identified by each workflow

and their overlaps. Percentages of tryptic and semi-tryptic precursors are indicated for each workflow. Only post-filtered data are shown (q-value < 0.01, each precursor was identified at least twice in at least one condition). B) Protein sequence coverage distribution for shared protein accessions across workflows and their overlaps. C) Raincloud plot showing the distribution of normalised precursor-level CVs for each workflow. The density curve represents the CV distribution, while the boxplot below indicates the median (line), interquartile range (box) and whiskers spreading to 1.5x the interquartile range. Individual points represent precursor-level CVs.

Comparison of FASTA-based and native semi-specific digestion strategies in DIA-NN for LiP-MS

We initially developed a workaround to enable semi-tryptic data analysis in DIA-NN (v2.2) by generating a semi-tryptic peptide FASTA file, prior to the implementation of the semi-specific digestion support in the new beta version of DIA-NN (v2.3). Although this workaround is no longer necessary from DIA-NN version 2.3 onwards, it remains a useful strategy for specialized applications, such as custom protease motifs (e.g., caspase motifs [38]) or proteases not supported by current search engines, as a fully semi-tryptic search would confer an unnecessary expansion of the search space. Furthermore, the full semi-tryptic FASTA file still enables semi-tryptic searches in the current stable release of DIA-NN (version 2.2), as well as with its older versions. We also benchmarked this workaround against the new semi-specific digestion option in DIA-NN (v2.3) (**Figure S3**). Substantial overlap was observed between workflows, and the FASTA-based approach in v2.2 achieved identification rates close to those obtained with the semi-specific option in v2.3. This confirms that the workaround remains valid, although the new semi-specific digestion feature outperforms this workaround and is recommended for future LiP-MS analyses.

Capturing conformational dynamics with DIA-LiPA: volcano plots and structural barcodes

We next examined the ability of each workflow to detect conformational changes using volcano plots and structural barcodes, the functional output of DIA-LiPA (**Figure 3**). All workflows identified FKBP1A with one or more significant precursor hits, confirming the known target of rapamycin. Interestingly, precursors that were significantly more abundant in the rapamycin-treated condition were tryptic, whereas those that were less abundant were semi-tryptic, suggesting a more shielded FKBP1A conformation upon rapamycin binding. Library-free DIA-NN additionally detected six precursors from other proteins, while empirical DIA-NN detected one.

However, these hits were single precursors near the significance thresholds and mapped to short stretches with low coverage (data not shown), suggesting likely false positives.

Structural barcodes below each volcano plot visualize differential, unchanged and missing peptides across the protein sequence. DIA-NN achieved broader FKBP1A coverage (88% library-free, 83% empirical) compared to Spectronaut (56% and 50%), enabling more distinct structural signatures. While the extra 5% coverage in library-free DIA-NN seems minor, zooming into precursor trypticity in the extended barcodes reveals additional dynamics (**Figure 4**). For example, around Trp59, a key residue in the rapamycin-binding pocket [39], the tryptic peptides was found at higher levels in the rapamycin condition, indicating shielding from PK cleavage. Semi-tryptic counterparts of this region are found at higher levels in the solvent condition, consistent with increased flexibility in the unbound state. Similarly, near Phe99, the tryptic peptide was not detected, but its semi-tryptic counterpart was found at higher levels in the unbound condition. These patterns provide compelling evidence of rapamycin binding, causing shielding and altered accessibility in these regions, and highlight DIA-LiPA's ability to capture conformational changes.

Including missingness in the structural barcodes adds interpretative value when classical quantitative comparison based on fold-change and significance testing is not possible. While statistical modelling of missingness is challenging, missing peptides are usually filtered out downstream or imputed [15,16]. Since imputation risks introducing bias and false positives [40], simply reporting absence can add interpretation value. For example, the first tryptic peptide has semi-tryptic counterparts and missing counterparts. In cases where peptides are detected in one condition but absent in the other, preventing quantitative comparison due to low abundance or search engine limitations, missingness patterns may still point to structural dynamics. Together, these results underscore the added value of semi-tryptics for probing conformational changes and demonstrate how DIA-LiPA integrates trypticity and missingness to deliver a more nuanced view of protein structural dynamics in DIA-based LiP-MS workflows.

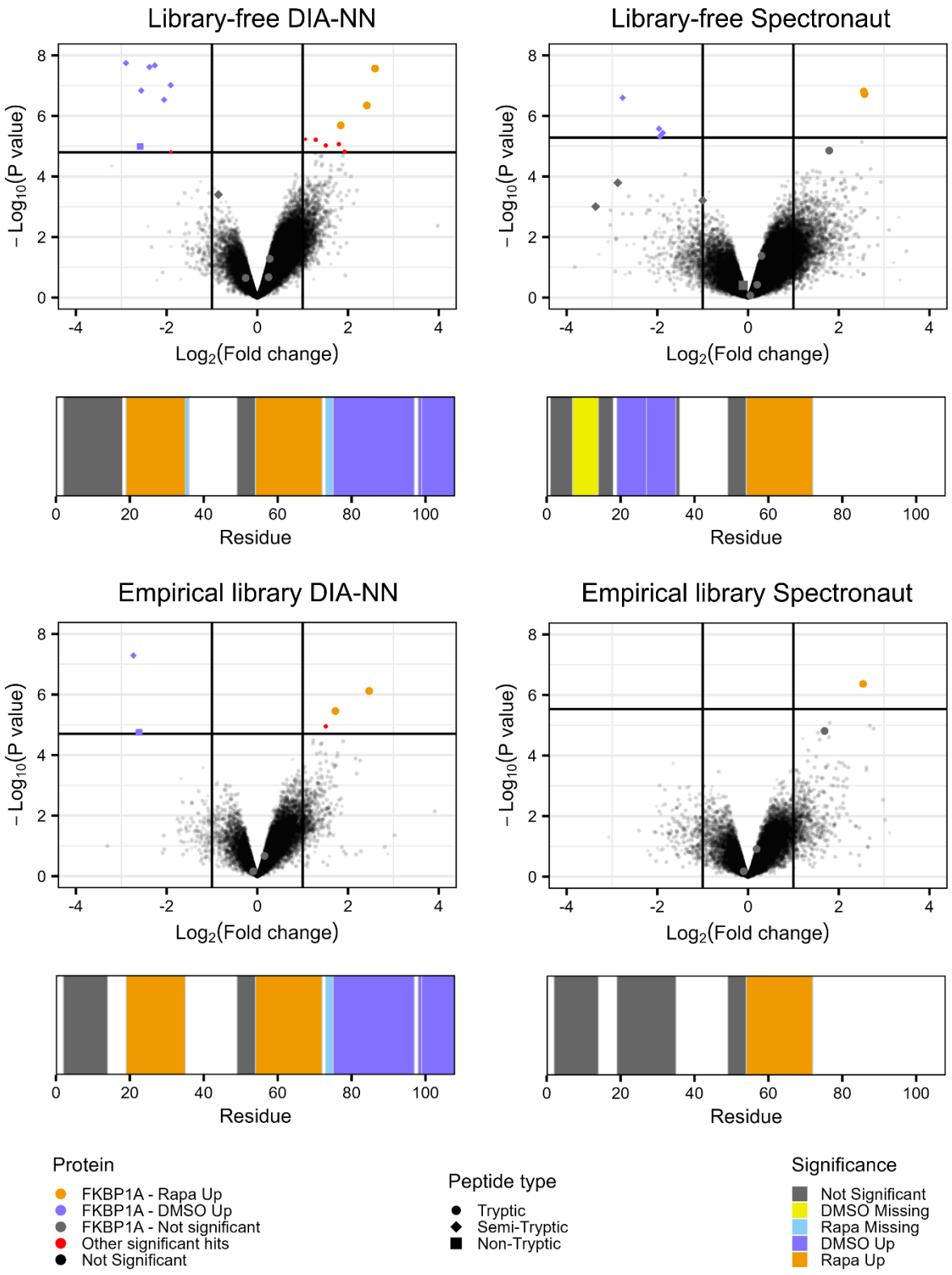

Figure 3: Downstream structural output of DIA LiP-MS workflows analysed with DIA-LiPA. Volcano plots show the differential abundance between rapamycin-treated versus solvent

control samples for each DIA workflow. Precursors are shaped by peptide type: circles (tryptic), diamonds (semi-tryptic), squares (non-tryptic). FKBP1A precursors are coloured by directionality: orange (significantly higher in rapamycin-treated), dark blue (significantly higher in solvent control), grey (not significant). Other significant hits appear in red; non-significant precursors in black. Significance thresholds: $|\log_2 FC| \geq 1$ and adjusted p-value ≤ 0.05. Below each volcano plot, a structural barcode summarizes FKBP1A results for that workflow. Each vertical bar represents a potential LiP precursor, coloured consistently: orange (significantly higher in rapamycin-treated), dark blue (significantly higher in solvent control), grey (unchanged), light blue (missing in rapamycin-treated), yellow (missing in solvent control), white (not detected).

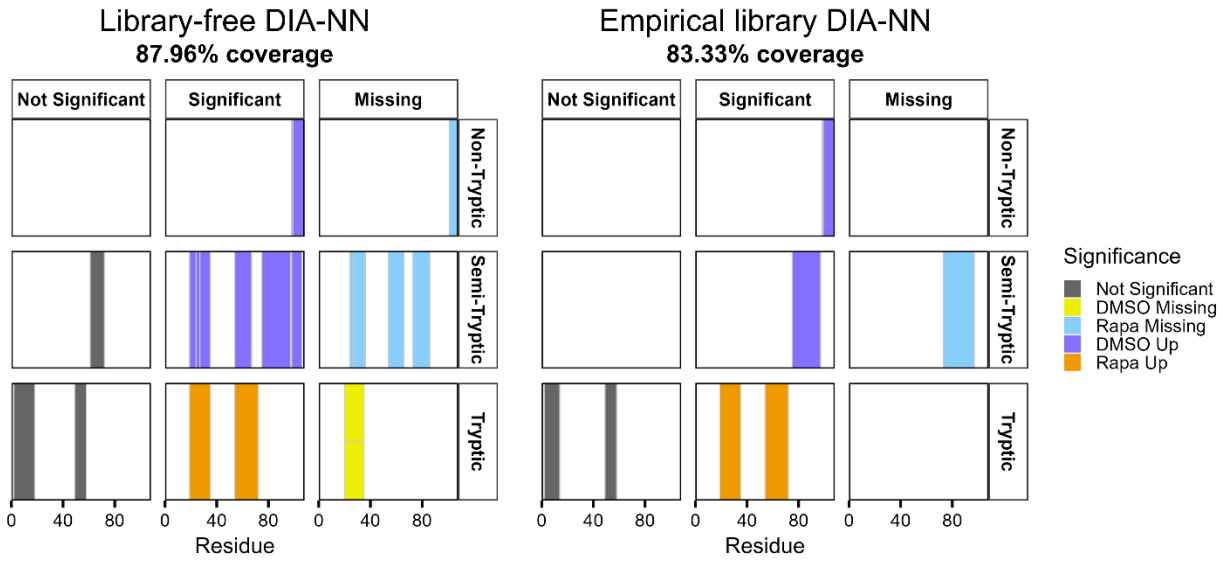

Figure 4: Extended structural barcodes for FKBP1A in library-free and empirical DIA-NN workflows. Each panel represents the FKBP1A sequence segmented by precursor trypticity (rows: tryptic, semi-tryptic, non-tryptic) and detection status (columns: not significant, significant, missing). Bars indicate precursor positions along the sequence, coloured by significance: orange (significantly higher in rapamycin-treated), dark blue (significantly higher in solvent control), grey (not significant), light blue (missing in rapamycin-treated), yellow (missing in solvent control), white (not detected). Bars are stacked when there are multiple precursors corresponding to the same peptide sequence. Coverage percentages for each workflow are shown above the barcodes. Significance thresholds match those of Figure 3 ($|\log_2 FC| \geq 1$ and adjusted p-value ≤ 0.05).

Validation of DIA-LiPA on yeast dataset

To demonstrate the generalizability and utility of DIA-LiPA, we reanalysed a publicly available yeast heat shock dataset [27] using two library-free workflows (DIA-NN and Spectronaut), followed by downstream analysis via DIA-LiPA.

Precursor identifications and overlaps between workflows demonstrate high consistency and comprehensive coverage, with both tryptic and semi-tryptic peptides contributing substantially (**Figure 5A**). Semi-tryptics represent roughly 40% of all identifications, indicating a lot of structural information in the dataset.

Structural barcodes for Hsp104 (**Figure 5B**), a key disaggregase highlighted in the original study, reveal domain-level regulation patterns across workflows. Compared to the original barcode, modern search engines detect more precursors, resulting in improved coverage and a more comprehensive structural readout. These barcodes align with the observations of Cappelletti *et al.*, who mapped altered peptides to ATP-binding sites, substrate channels and solvent-exposed regions and suggested that multiple structural states coexist in the sample. While their fractionation approach (soluble versus insoluble) was designed to disentangle these states, our DIA-LiPA analysis of total lysates alone recapitulates these insights and adds clarity on domain-specific changes. For example, the expanded barcode demonstrates that the middle region (MD) contains both significantly downregulated tryptics and semi-tryptics upon heat shock, consistent with a region that is simultaneously flexible and involved in aggregation interfaces, supporting its role in modulating substrate threading and ATPase activity during heat shock [41,42]. This aligns well with the notion that multiple structural states can coexist.

Volcano plots (**Figure 5C**) provide a global view of structural dynamics, based on precursors consistently detected across both conditions. Tryptic precursors exhibit a pronounced shift toward negative fold changes, even after adjustment for protein-level fold changes in the trypsin control samples, indicating reduced abundance after heat shock. This likely reflects increased proteolytic accessibility due to unfolding, leading to more cleavage events and consequently lower tryptic peptide abundance. In an ideal detection scenario, semi-tryptic counterparts would be consistently observed and exhibit a complementary shift toward positive fold changes. However, volcano plots only include precursors for which a statistical comparison is possible, i.e. those with detectable values in both conditions. Precursors that are completely missing from one condition cannot be assigned a p-value and are therefore excluded from the plot. This is relevant for semi-tryptic peptides, which are generated from regions that are surface-accessible to the protease. If a region, such as a buried hydrophobic core, becomes accessible only upon heat shock, the corresponding semi-tryptic peptides will be absent in the control condition and thus not represented in the volcano

plot. This highlights the added value of integrating missingness patterns to detect structural changes beyond the protein surface.

Together, these findings confirm that DIA-LiPA enhances interpretability of existing datasets and uncovers additional structural insights, offering a powerful resource for the structural proteomics community.

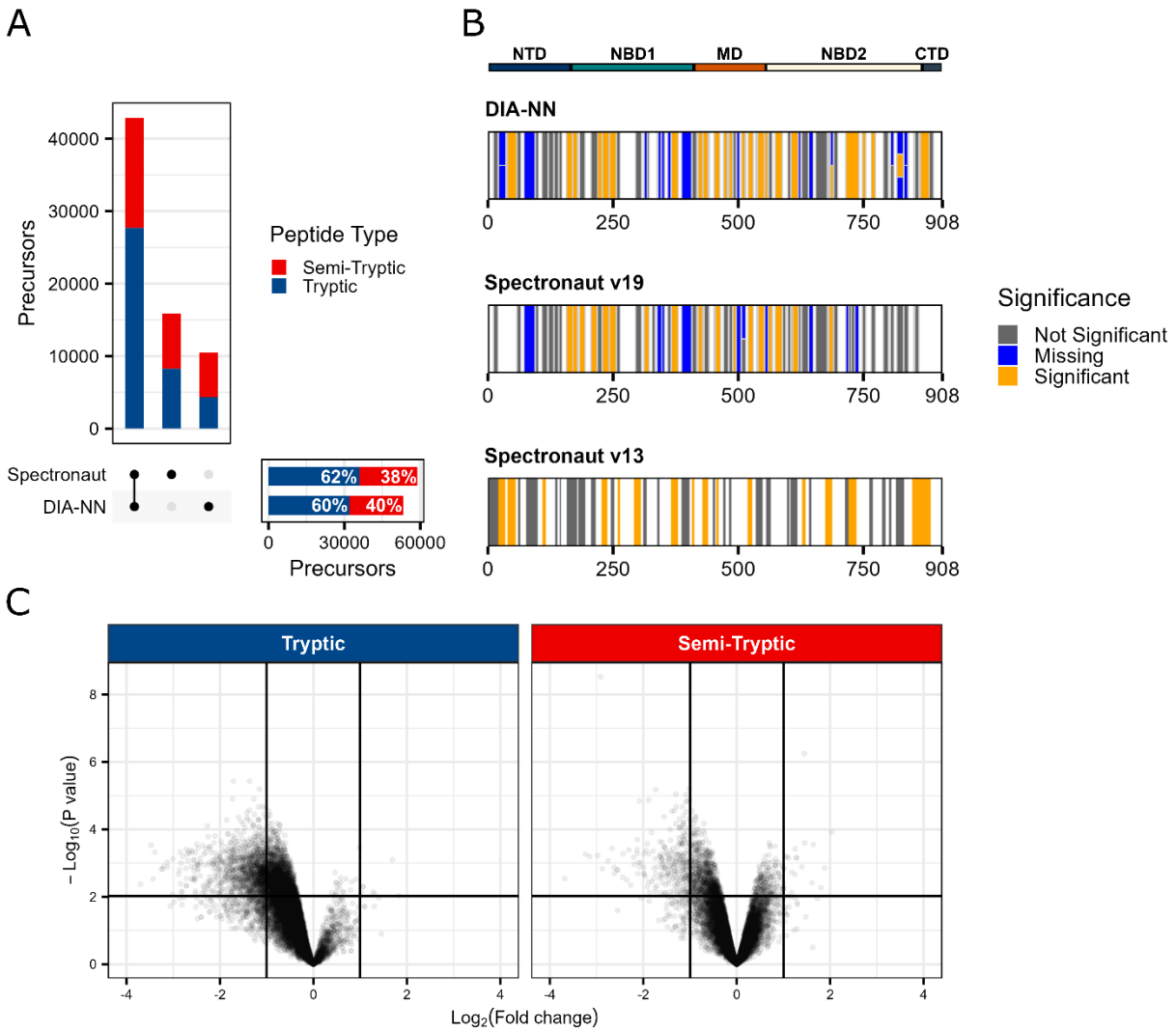

Figure 5: Validation of DIA-LiPA on the yeast heat shock dataset. A) UpSet plot showing the absolute number of precursors identified by library-free DIA-NN and Spectronaut workflows and their overlaps. Percentages of tryptic and semi-tryptic precursors are indicated for each workflow. Only post-filtered data are shown (q-value < 0.01, each precursor was identified at least twice in at least one condition). B) Structural barcodes of Hsp104, a highlighted target in the original study, for both workflows alongside the original barcode from the study. Each vertical bar represents a

potential LiP precursor, coloured by significance: orange (significant), blue (missing), grey (not significant), white (not detected by MS). Bars are stacked when there are multiple precursors corresponding to the same peptide sequence. Protein domains (N-terminal domain; NTD, nucleotide-binding domain 1; NBD1, middle domain; MD, nucleotide-binding domain 2; NBD2, C-terminal domain; CTD) are indicated on top. C) Volcano plots separated by precursor trypticity. Left: tryptic precursors; right: semi-tryptic precursors. Each point represents a precursor. Significance thresholds are indicated by vertical and horizontal lines: $|\log_2 FC| \geq 1$ and adjusted p-value ≤ 0.05.

Conclusions

Our findings illustrate how recent advances in machine learning have transformed DIA workflows, making library-free approaches not only sufficient but often superior to traditional DDA-based libraries. This shift reduces experimental overhead, instrument time and sample requirements, critical advantages for applications with limited material such as clinical biopsies.

In this context, we introduce DIA-LiPA, a pipeline tailored for LiP-MS that integrates semi-tryptic peptides and uniquely accounts for missingness to enable a more nuanced structural interpretation, revealing subtle conformational changes with high confidence. These capabilities extend beyond peptide quantification, offering a framework for mechanistic insights into protein dynamics.

While benchmarking DIA-NN's new semi-specific digestion option confirms its robustness, the broader impact of this work lies in demonstrating how DIA-LiPA leverages these advances to deliver reproducible, high-resolution structural information. Validation across two datasets, namely the rapamycin-treated human cell lysate and yeast heat shock, shows that DIA-LiPA not only reproduces known structural signatures but also uncovers additional layers of regulation. Together, these findings position DIA-LiPA as a valuable addition to the LiP-MS toolbox and a step toward more accessible, high-confidence structural proteomics. Furthermore, we also provide an alternative search strategy including a semi-tryptic FASTA file which may be adapted based on the provided scripts to serve applications outside of LiP-MS.

Author Contributions

All authors contributed to the final version of the manuscript. ‡CVL and EA contributed equally to this work.

Funding Sources

EA is a PhD fellow from The Research Foundation – Flanders (FWO), project number 1177425N. KG acknowledges support from The Research Foundation – Flanders (FWO), project numbers 860960 IBOF-23-005 and G002721N, and from the Special Research Fund of Ghent University, project BOF/24J/2023/152.

Notes

The authors declare no competing financial interest.

Acknowledgement

We acknowledge the VIB Proteomics Core for their support in performing the mass spectrometry measurements. We also thank Ludovic Gillet and Paola Picotti (ETH Zurich) for providing initial expertise and guidance on the LiP-MS protocol.

References

(1) Nussinov, R.; Liu, Y.; Zhang, W.; Jang, H. Protein Conformational Ensembles in Function: Roles and Mechanisms. *RSC Chem. Biol.* **2023**, *4*, 850–864.

(2) Ramanathan, A.; Savol, A.; Burger, V.; Chennubhotla, C. S.; Agarwal, P. K. Protein Conformational Populations and Functionally Relevant Substates. *Acc. Chem. Res.* **2013**, *47*, 149–156.

(3) Tobi, D.; Bahar, I. Structural Changes Involved in Protein Binding Correlate with Intrinsic Motions of Proteins in the Unbound State. *Proc. Natl. Acad. Sci. U. S. A.* **2005**, *102*, 18908–18913.

(4) Schweizer, L.; Mueller, L. Protein Conformational Dynamics and Signaling in Evolution and Pathophysiology. *Biased Signal. Physiol. Pharmacol. Ther.* **2014**, 209–249.

(5) Chavez, J. D.; Bruce, J. E. Chemical Cross-Linking with Mass Spectrometry: A Tool for Systems Structural Biology. *Curr. Opin. Chem. Biol.* **2019**, *48*, 8–18.

(6) Yu, C.; Huang, L. Cross-Linking Mass Spectrometry (XL-MS): An Emerging Technology for Interactomics and Structural Biology. *Anal. Chem.* **2017**, *90*, 144.

(7) Vinciauskaite, V.; Masson, G. R. Fundamentals of HDX-MS. *Essays Biochem.* **2023**, *67*, 301–

314.

(8) Savitski, M. M.; Reinhard, F. B. M.; Franken, H.; Werner, T.; Savitski, M. F.; Eberhard, D.; Molina, D. M.; Jafari, R.; Dovega, R. B.; Klaeger, S.; Kuster, B.; Nordlund, P.; Bantscheff, M.; Drewes, G. Tracking Cancer Drugs in Living Cells by Thermal Profiling of the Proteome. *Science.* **2014**, *346*.

(9) Franken, H.; Mathieson, T.; Childs, D.; Sweetman, G. M. A.; Werner, T.; Tögel, I.; Doce, C.; Gade, S.; Bantscheff, M.; Drewes, G.; Reinhard, F. B. M.; Huber, W.; Savitski, M. M. Thermal Proteome Profiling for Unbiased Identification of Direct and Indirect Drug Targets Using Multiplexed Quantitative Mass Spectrometry. *Nat. Protoc.* **2015**, *10*, 1567–1593.

(10) Li, K.; Chen, S.; Wang, K.; Wang, Y.; Xue, L.; Ye, Y.; Fang, Z.; Lyu, J.; Zhu, H.; Li, Y.; Yu, T.; Yang, F.; Zhang, X.; Guo, S.; Ruan, C.; Zhou, J.; Wang, Q.; Dong, M.; Luo, C.; Ye, M. A Peptide-Centric Local Stability Assay Enables Proteome-Scale Identification of the Protein Targets and Binding Regions of Diverse Ligands. *Nat. Methods* **2025**, *22*, 278–282.

(11) Feng, Y.; De Franceschi, G.; Kahraman, A.; Soste, M.; Melnik, A.; Boersema, P. J.; De Laureto, P. P.; Nikolaev, Y.; Oliveira, A. P.; Picotti, P. Global Analysis of Protein Structural Changes in Complex Proteomes. *Nat. Biotechnol.* **2014**, *32*, 1036–1044.

(12) Happonen, L. J.; Varjosalo, M. State-of-the-Art and Future Directions in Structural Proteomics. *Mol. Cell. Proteomics* **2025**, 101065.

(13) Lu, H.; Zhu, Z.; Fields, L.; Zhang, H.; Li, L. Mass Spectrometry Structural Proteomics Enabled by Limited Proteolysis and Cross-Linking. *Mass Spectrom. Rev.* **2024**, 1–28.

(14) Batth, T. S.; Locard-Paulet, M.; Doncheva, N. T.; Lopez Mendez, B.; Jensen, L. J.; Olsen, J. V. Streamlined Analysis of Drug Targets by Proteome Integral Solubility Alteration Indicates Organ-Specific Engagement. *Nat. Commun.* **2024**, *15*, 1–17.

(15) Schopper, S.; Kahraman, A.; Leuenberger, P.; Feng, Y.; Piazza, I.; Müller, O.; Boersema, P. J.; Picotti, P. Measuring Protein Structural Changes on a Proteome-Wide Scale Using Limited Proteolysis-Coupled Mass Spectrometry. *Nat. Protoc.* **2017**, *12*, 2391–2410.

(16) Malinovska, L.; Cappelletti, V.; Kohler, D.; Piazza, I.; Tsai, T. H.; Pepelnjak, M.; Stalder, P.; Dörig, C.; Sesterhenn, F.; Elsässer, F.; Kralickova, L.; Beaton, N.; Reiter, L.; de Souza, N.; Vitek, O.; Picotti, P. Proteome-Wide Structural Changes Measured with Limited Proteolysis-Mass Spectrometry: An Advanced Protocol for High-Throughput Applications. *Nat. Protoc.* **2023**, *18*, 659–682.

(17) Koudelka, T.; Bassot, C.; Piazza, I. Benchmarking of Quantitative Proteomics Workflows for Limited Proteolysis Mass Spectrometry. *Mol. Cell. Proteomics* **2025**, *24*, 100945.

(18) Staes, A.; Mendes Maia, T.; Dufour, S.; Bouwmeester, R.; Gabriels, R.; Martens, L.; Gevaert, K.; Impens, F.; Devos, S. Benefit of In Silico Predicted Spectral Libraries in Data-Independent Acquisition Data Analysis Workflows. *J. Proteome Res.* **2024**, *23*, 2078–2089.

(19) Lou, R.; Cao, Y.; Li, S.; Lang, X.; Li, Y.; Zhang, Y.; Shui, W. Benchmarking Commonly Used Software Suites and Analysis Workflows for DIA Proteomics and Phosphoproteomics. *Nat.*

Commun. **2023**, *14*, 1–17.

(20) Demichev, V.; Messner, C. B.; Vernardis, S. I.; Lilley, K. S.; Ralser, M. DIA-NN: Neural Networks and Interference Correction Enable Deep Proteome Coverage in High Throughput. *Nat. Methods* **2019**, *17*, 41–44.

(21) Bruderer, R.; Bernhardt, O. M.; Gandhi, T.; Miladinović, S. M.; Cheng, L. Y.; Messner, S.; Ehrenberger, T.; Zanotelli, V.; Butscheid, Y.; Escher, C.; Vitek, O.; Rinner, O.; Reiter, L. Extending the Limits of Quantitative Proteome Profiling with Data-Independent Acquisition and Application to Acetaminophen-Treated Three-Dimensional Liver Microtissues. *Mol. Cell. Proteomics* **2015**, *14*, 1400–1410.

(22) Wen, B.; Freestone, J.; Riffle, M.; MacCoss, M. J.; Noble, W. S.; Keich, U. Assessment of False Discovery Rate Control in Tandem Mass Spectrometry Analysis Using Entrapment. *Nat. Methods* **2025**, *22*, 1454–1463.

(23) Quast, J. P.; Schuster, D.; Picotti, P. Protti: An R Package for Comprehensive Data Analysis of Peptide- and Protein-Centric Bottom-up Proteomics Data. *Bioinforma. Adv.* **2022**, *2*.

(24) Nagel, L.; Grossbach, J.; Cappelletti, V.; Dörig, C.; Picotti, P.; Beyer, A. Analysis of Limited Proteolysis-Coupled Mass Spectrometry Data. *Mol. Cell. Proteomics* **2025**, *24*, 100934.

(25) Chiva, C.; Olivella, R.; Borràs, E.; Espadas, G.; Pastor, O.; Solé, A.; Sabidó, E. QCloud: A Cloud-Based Quality Control System for Mass Spectrometry-Based Proteomics Laboratories. *PLoS One* **2018**, *13*, e0189209.

(26) Olivella, R.; Chiva, C.; Serret, M.; Mancera, D.; Cozzuto, L.; Hermoso, A.; Borràs, E.; Espadas, G.; Morales, J.; Pastor, O.; Solé, A.; Ponomarenko, J.; Sabidó, E. QCloud2: An Improved Cloud-Based Quality-Control System for Mass-Spectrometry-Based Proteomics Laboratories. *J. Proteome Res.* **2021**, *20*, 2010–2013.

(27) Cappelletti, V.; Hauser, T.; Piazza, I.; Pepelnjak, M.; Malinovska, L.; Fuhrer, T.; Li, Y.; Dörig, C.; Boersema, P.; Gillet, L.; Grossbach, J.; Dugourd, A.; Saez-Rodriguez, J.; Beyer, A.; Zamboni, N.; Caflisch, A.; de Souza, N.; Picotti, P. Dynamic 3D Proteomes Reveal Protein Functional Alterations at High Resolution in Situ. *Cell* **2021**, *184*, 545-559.e22.

(28) Kong, A. T.; Leprevost, F. V.; Avtonomov, D. M.; Mellacheruvu, D.; Nesvizhskii, A. I. MSFragger: Ultrafast and Comprehensive Peptide Identification in Mass Spectrometry–Based Proteomics. *Nat. Methods* **2017**, *14*, 513–520.

(29) Banaszynski, L. A.; Liu, C. W.; Wandless, T. J. Characterization of the FKBP·Rapamycin·FRB Ternary Complex. *J. Am. Chem. Soc.* **2005**, *127*, 4715–4721.

(30) Piazza, I.; Beaton, N.; Bruderer, R.; Knobloch, T.; Barbisan, C.; Chandat, L.; Sudau, A.; Siepe, I.; Rinner, O.; de Souza, N.; Picotti, P.; Reiter, L. A Machine Learning-Based Chemoproteomic Approach to Identify Drug Targets and Binding Sites in Complex Proteomes. *Nat. Commun.* **2020**, *11*, 1–13.

(31) Reber, V.; Gstaiger, M. Target Deconvolution by Limited Proteolysis Coupled to Mass Spectrometry. *Methods Mol. Biol.* **2023**, *2706*, 177–190.

(32) Fahrner, M.; Kook, L.; Fröhlich, K.; Biniossek, M. L.; Schilling, O. A Systematic Evaluation of Semispecific Peptide Search Parameter Enables Identification of Previously Undescribed N-Terminal Peptides and Conserved Proteolytic Processing in Cancer Cell Lines. *Proteomes* **2021**, *9*, 26.

(33) Alves, P.; Arnold, R. J.; Clemmer, D. E.; Li, Y.; Reilly, J. P.; Sheng, Q.; Tang, H.; Xun, Z.; Zeng, R.; Radivojac, P. Fast and Accurate Identification of Semi-Tryptic Peptides in Shotgun Proteomics. *Bioinformatics* **2008**, *24*, 102–109.

(34) Barkovits, K.; Pacharra, S.; Pfeiffer, K.; Steinbach, S.; Eisenacher, M.; Marcus, K.; Uszkoreit, J. Reproducibility, Specificity and Accuracy of Relative Quantification Using Spectral Library-Based Data-Independent Acquisition. *Mol. Cell. Proteomics* **2019**, *19*, 181.

(35) Staes, A.; Mendes Maia, T.; Dufour, S.; Bouwmeester, R.; Gabriels, R.; Martens, L.; Gevaert, K.; Impens, F.; Devos, S. Benefit of In Silico Predicted Spectral Libraries in Data-Independent Acquisition Data Analysis Workflows. *J. Proteome Res.* **2024**, *23*, 2078–2089.

(36) Katsavelis, D.; van der Hart, M. G. C.; Wolters, J. C.; Permentier, H. P.; Horvatovich, P.; Cremers, T. I. F. H. Impact of Sample Preparation Strategies on the Quantitative Accuracy of Low-Abundance Serum Proteins in Shotgun Proteomics. *J. Proteome Res.* **2025**, *24*, 4792–4803.

(37) Ma, R.; Meng, H.; Wiebelhaus, N.; Fitzgerald, M. C. Chemo-Selection Strategy for Limited Proteolysis Experiments on the Proteomic Scale. *Anal. Chem.* **2018**, *90*, 14039.

(38) Julien, O.; Wells, J. A. Caspases and Their Substrates. *Cell Death Differ.* **2017**, *24*, 1380–1389.

(39) DeCenzo, M. T.; Park, S. T.; Jarrett, B. P.; Aldape, R. A.; Futer, O.; Murcko, M. A.; Livingston, D. J. FK506-Binding Protein Mutational Analysis: Defining the Active-Site Residue Contributions to Catalysis and the Stability of Ligand Complexes. *Protein Eng.* **1996**, *9*, 173–180.

(40) Liu, M.; Dongre, A. Proper Imputation of Missing Values in Proteomics Datasets for Differential Expression Analysis. *Brief. Bioinform.* **2021**, *22*, 1–17.

(41) DeSantis, M. E.; Sweeny, E. A.; Snead, D.; Leung, E. H.; Go, M. S.; Gupta, K.; Wendler, P.; Shorter, J. Conserved Distal Loop Residues in the HSP104 and CLPB Middle Domain Contact Nucleotide-Binding Domain 2 and Enable Hsp70-Dependent Protein Disaggregation. *J. Biol. Chem.* **2014**, *289*, 848–867.

(42) Heuck, A.; Schitter-Sollner, S.; Józef Suskiewicz, M.; Kurzbauer, R.; Kley, J.; Schleiffer, A.; Rombaut, P.; Herzog, F.; Clausen, T. Structural Basis for the Disaggregase Activity and Regulation of Hsp104. *Elife* **2016**, *5*, e21516.